J Nanopart Res (2015) 17:94
DOI 10.1007/s11051-015-2902-z

RESEARCH PAPER

Visible light-driven photocatalytic degradation of the organic pollutant methylene blue with hybrid palladium–fluorine-doped titanium oxide nanoparticles

Sonia Lázaro-Navas · Sanjiv Prashar · Mariano Fajardo · Santiago Gómez-Ruiz

Received: 10 September 2014 / Accepted: 2 February 2015 / Published online: 13 February 2015

Abstract The synthesis of mesoporous aggregates of titanium oxide nanoparticles (F0) is described using a very cheap and simple synthetic protocol. This consists of the reaction of titanium tetraisopropoxide and a solution of HNO_3 in water (pH 2.0) and subsequent filtration. In addition, fluorine-doped titanium oxides (F1, F2, F5 and F10) were synthesized using the same method, adding increasing amounts of NaF to the reaction mixture (avoiding the use of expensive reagents such as NH_4F or trifluoroacetic acid). The resulting materials were calcined at different temperatures (500, 600 and 650 °C) giving particles sized between 10 and 20 nm. Furthermore, a hybrid F-doped TiO_2 with supported palladium nanoparticles of ca. 20 nm (F5-500-Pd1) was synthesized by grafting an organometallic palladium(II) salt namely $[Pd(cod)Cl_2]$ (cod = 1,5-cyclooctadiene). Photocatalytic studies of the degradation of methylene blue (MB) were carried out under UV light using all the synthesized material (non-doped an F-doped TiO_2), observing that the increase in the quantity of fluorine has a positive effect on the photocatalytic activity. F5-500 is apparently the material which has the most convenient structural properties (in terms of surface area and anatase/rutile ratio) and thus a higher photocatalytic activity. The hybrid material F-doped TiO_2–Pd nanoparticles (F5-500-Pd1) has a lower band gap value than F5-500, and thus photocatalytic degradation of MB under LED visible light was achieved using F5-500-Pd1 as photocatalyst.

Keywords Titania nanoparticles · Pd nanoparticles · Environmental applications · Pollutant degradation

Introduction

Heterogeneous photocatalysis is an "advanced oxidation process" (AOP) and has emerged as an efficient technology to eliminate a high number of chemical compounds in water and air (Glaze et al. 1987; Teichner 2008; Umadevi et al. 2014). A photocatalytic reaction begins when a semiconductor is irradiated with photons having the same or higher energy than that of its band gap. At this moment, electrons and holes are generated in the conduction and valence bands (VB), respectively, and migrate to the TiO_2 surface. Normally, an electron is promoted to the conduction band (CB) and a positive hole is formed in the VB. However, in the excited state, electrons and holes can be recombined and thus a dissipation of the

Electronic supplementary material The online version of this article (doi:10.1007/s11051-015-2902-z) contains supplementary material, which is available to authorized users.

S. Lázaro-Navas · S. Prashar · M. Fajardo · S. Gómez-Ruiz (✉)
Departamento de Biología y Geología, Física y Química Inorgánica, ESCET, Universidad Rey Juan Carlos, Calle Tulipán s/n, 28933 Móstoles, Madrid, Spain
e-mail: santiago.gomez@urjc.es

input energy as heat can occur. Nevertheless, a reaction of some electron donors and/or electron acceptors with the compounds adsorbed on the semiconductor surface may lead to their degradation (Herrmann et al. 2007; Sánchez-Muñoz et al. 2013). Degradation processes require the formation of radicals $OH^{\cdot}$, O^{2-}, H_2O_2 or O_2, which play an important role in the photodecomposition of organic compounds and are able (in a complete model reaction) to form CO_2 and water (Sánchez-Muñoz et al. 2013).

For the degradation of chemicals, different semiconductors can be used as photocatalysts, such as ZnO, CdS, Fe_2O_3 and WO_3. However, titanium oxide (TiO_2) is one of the functional metal oxide semiconductors that perform with high efficiency in photocatalysis due to its non-toxicity, low cost, excellent energy conversion and long-term chemical stability (Bayarri et al. 2005; Vivero-Escoto et al. 2012; Umadevi et al. 2014).

Titanium oxide has three crystalline forms: anatase (band gap of 3.23 eV), rutile (band gap of 3.02 eV) and brookite. Among these crystalline forms, anatase is the crystalline form with the best photocatalytic properties (Luttrell et al. 2014), due to its high surface area and low tendency for electron–hole pair recombination. The rutile phase is the most thermodynamically stable, whereas brookite and anatase are metastable and transformed to rutile on heating.

In recent years, a scientific and engineering interest in TiO_2 has grown due to its electric and optical properties, and its high chemical stability makes it a very good candidate for numerous applications (Vivero-Escoto et al. 2012). Titanium oxide is effective as a component of bone implants due to its high biocompatibility, (Diebold 2003) and in other electronic devices or in coatings due to its optical properties (Diebold 2003). In addition, Titanium oxide can also be used for hydrogen production by water splitting (Kudo and Miseki 2009), or for nitrogen fixing (Cherchi and Gu 2010). Titanium oxide can be applied to air or water purification, odour elimination, or in contaminated soils (Herrmann et al. 2007). With regards to water purification, TiO_2 has a great potential for different processes including disinfection, organic compound degradation, pharmaceutical compound degradation and heavy metal deposition [Pt(IV), Au(III) and Rh(III)] (Hoffmann et al. 1995).

The photocatalytic efficiency of titanium oxide-based materials is favoured by an increase of the surface area and the crystallinity (Vivero-Escoto et al. 2012; Sánchez-Muñoz et al. 2013). These two properties are normally present in mesoporous TiO_2 or mesoporous aggregates of titanium oxides; thus, a higher photocatalytic activity is normally expected for porous systems on direct comparison to non-porous TiO_2. However, it is very difficult to prepare mesoporous TiO_2 materials containing highly crystalline anatase walls and a large surface area. During the past decade, different synthetic methods have been extensively studied to prepare mesoporous/nanoporous TiO_2 films or particles with or without the use of organic surfactant templates, hydrothermal syntheses, or using sol–gel methods (Chen and Mao 2007; Sánchez-Muñoz et al. 2013).

To enhance the photocatalytic properties of TiO_2 materials, a band gap reduction is also necessary, as this usually increases the applicability and efficiency using visible light sources instead of UV light. Band gap reduction is generally achieved by doping with one element, several elements, or with an element and a co-catalyst (Tan et al. 2011; Chen and Mao 2007; Yu et al. 2002; Zaleska 2008). Metal-doping was the dominant methodology at the initial stage in the study of the effect of doping on the photocatalytic properties of TiO_2. It was reported that the introduction of metal ions into the TiO_2 matrix may significantly influence the photoactivity, charge recombination rates and interfacial electron transfer (Cui et al. 2008). However, the metal-doping of TiO_2 photocatalysts also has some drawbacks, such as thermal instability and an increase of the electron–hole recombination. On the other hand, nonmetal-doped TiO_2 seem to be more promising candidates in photocatalytic reactions and among them N doped TiO_2 has been the most studied although other elements such as B, C, F, P, S, or I have also been reported (Cui et al. 2008).

With regards to doping with F, the formation of ultrareactive (001) faces is one of the most interesting advantages reported recently. Thus, Yu et al. prepared F-doped TiO_2 by hydrolysis of titanium tetraisopropoxide in a mixed NH_4F-H_2O solution. The use of F-doping not only improved the crystallinity of anatase but also suppressed the formation of the brookite phase and prevented the phase transition of anatase to rutile (Yu et al. 2002). In addition, it was confirmed that F-doping in TiO_2 induces visible light-driven photocatalysis by the creation of oxygen vacancies (Li et al. 2005). F-doping in TiO_2 can also convert Ti^{4+} to Ti^{3+} by charge compensation and the existence of Ti^{3+} can reduce the electron–hole recombination rate and subsequently enhance the photocatalytic activity (Umadevi et al. 2014).

In this context, the simple synthetic method for the preparation of mesoporous aggregates of titanium oxide described previously by our group (Sánchez-Muñoz et al. 2013) has been modified by the incorporation of F using a cheap fluorine source such as NaF, instead of other more hazardous and expensive reagents such as trifluoroacetic acid, to prepare F-doped mesoporous aggregates of titanium oxide which have been characterized using different techniques. In addition, in contrast to most of the reported methods, our synthetic procedure does not need the use of a surfactant or the formation of a sol for the preparation of nanostructured titanium oxide.

In a final step, we have used the titanium oxide-based materials as photocatalyst in the degradation of methylene blue (MB), because this pollutant is commonly used as a dye in textile, polymeric, cosmetics, pharmaceutical and food industries and its presence in waste waters is very common and can result in problems such as chemical oxygen demand (COD) and high toxicity to flora and fauna if the water is not properly treated (Mohammed et al. 2014). Thus, in our study, we have observed a higher photocatalytic activity under UV light with increasing quantities of superficial F. In addition, a hybrid F-doped TiO_2 with supported palladium nanoparticles (F5-500-Pd1) was synthesized by grafting the organometallic palladium(II) salt [$Pd(cod)Cl_2$] (cod = 1,5-cyclooctadiene). The co-doped hybrid material was able to degrade MB under visible light with moderate photocatalytic activity. These results, obtained using visible light, are promising to increase the energetic efficiency of the degradation process which is much higher when using visible light compared with UV light (Yang et al. 2014) and can be an alternative to the current methods of treatment of MB, which are normally based on more expensive protocols such as adsorption (Mohammed et al. 2014), chemical oxidation (Wang 2008), foam flotation (Yue et al. 2008), electrolysis (Jin et al. 2003) and electro-coagulation (Sami and Bagani 2012).

Materials and methods

General remarks

N_2 gas adsorption–desorption isotherms were recorded using a Micrometrics ASAP 2020 analyzer, degassing previously the samples at 350 °C during 10 h. X-ray diffraction (XRD) patterns of the materials were obtained on a Philips Diffractometer model PW3040/00 ẊPert MPD/MRD at 45 kV and 40 mA, using wavelength CuKα ($\lambda = 1.5419$ Å) and using a high-angle measurement between 2θ 10°–100°. The mean crystallite size (D) was calculated from the line broadening of the corresponding XRD peaks, according to Scherrer equation (Danilchenko et al. 2002). ^{19}F NMR spectra were recorded on a Varian-Infinity Plus Spectrometer at 400 MHz operating at 2000 rpm. UV–Vis spectra were recorded using a Varian Cary 500 scan in diffuse reflectance mode and transformed to a magnitude proportional to the extinction coefficient (K) by means of the Kubelka–Munk function [$F(R_\infty)$], which was used for the calculation of the band gap. Conventional transmission electron microscopy (TEM) was carried out with a TECNAI 20 Philips, operating at 200 kV. Particle size distribution was determined by *Image J* software using the pixels of the TEM images. Processing of data for the calculation of the distribution was performed with *OriginPro 6.1* software.

Titanium(IV) tetraisopropoxide 97 % (Sigma-Aldrich), HNO_3 65 % (Sigma-Aldrich), NaF (Acros Organics), 2-propanol (Sigma-Aldrich), toluene (SDS) and MB (Scharlau) were used without further purification. Milli-Q water (18.2 MΩ cm) was used in all syntheses.

Synthesis of nano-sized mesoporous aggregates of TiO_2

Mesoporous aggregates of TiO_2 were prepared by controlled hydrolysis of titanium(IV) isopropoxide in a solution of HNO_3 in Milli-Q water at pH 2, without using surfactants or structure templates. This synthetic method is based on that developed by our group (Sánchez-Muñoz et al. 2013). Thus, in a typical synthesis, a 40-mL aliquot of titanium(IV) isopropoxide was dissolved in dry 2-propanol (2:5) and the solution was added dropwise to a solution of HNO_3 (500 mL) in Milli-Q water at pH 2 (adjusted with HNO_3) using a peristaltic pump for 10 min. After continuous stirring at room temperature for 16 h, the suspension was filtered and the resulting solid was dried at 90 °C. Finally, the material was separated into three parts and calcined in air in a Carbolite AAF 1100 furnace at 500, 600 or 650 °C for 16 h with a heating

rate of 0.8 °C/min. The resulting materials were named F0-500, F0-600 and F0-650, respectively.

Synthesis of fluorine-doped nano-sized mesoporous TiO_2

A 40-mL aliquot of titanium(IV) isopropoxide was dissolved in dry 2-propanol (2:5) and the solution was added dropwise to a solution of HNO_3 (500 mL) in Milli-Q water at pH 2 (adjusted with HNO_3) using a peristaltic pump for 10 min. At the same time, a solution of increasing amounts of NaF (0.22 g for F1 (1 %), 0.44 g for F2 (2 %), 1.10 g for F5 (5 %), and 2.21 g for F10 (10 %) in 100 mL of Milli-Q water was also added dropwise to the solution of HNO_3. After continuous stirring at room temperature for 16 h, the mixture was filtered and washed several times using Milli-Q water. The resulting solid was then dried at 90 °C. Finally, each material was separated into three parts and calcined in air in a Carbolite AAF 1100 furnace at 500, 600 or 650 °C for 16 h with a heating rate of 0.8 °C/min. The resulting materials were named F1-500, F1-600, F1-650, F2-500, F2-600, F2-650, F5-500, F5-600, F5-650, F10-500, F10-600 and F10-650.

Synthesis of hybrid F-doped TiO_2-Pd nanoparticles

Hybrid F-doped TiO_2 with supported palladium nanoparticles was synthesized by grafting of a Pd organometallic salt [Pd(cod)Cl_2]. A solid mixture of 27 mg of [Pd(cod)Cl_2] and 1.0 g of F5-500 was introduced into a Schlenk tube under an inert atmosphere. Then, toluene (100 mL) was added and the solution was stirred at 120 °C for 48 h. The solvents of the suspension were removed by filtration, and the solid was washed several times using toluene and Milli-Q water and the resulting solid was then dried at 100 °C. The material was named F5-500-Pd1.

Photocatalytic degradation of aqueous MB

For the photocatalytic experiments under UV light, 25 mg or 15 mg of the TiO_2 samples was dispersed in 50 mL of a 0.01 mM MB solution. The light source was a 6 W Hg tube lamp operating at 365 nm in a black box with a multi-stirrer (OVAN MM90) where the suspensions were located for the experiments. Prior to irradiation, suspensions with the photocatalyst were stirred for 1 h to ensure that the surface of the photocatalyst was saturated with MB (adsorption–desorption equilibrium). The total exposition under UV light of all experiments was 2 h. The degradation of organic dyes was monitored by measuring the absorbance every 15 min with a spectrophotometer (SP-830) at 660 nm wavelength, which is the maximum of the MB absorbance. All experiments were carried out in duplicate and the absorbance was measured in triplicate.

For the hybrid F-doped TiO_2–Pd nanoparticles photocatalytic experiment, 25 mg of the TiO_2 sample was dispersed in 50 mL of a 0.01 mM MB solution. The radiation source was a visible LED lamp (AS-Schwabe 42411, 4.5 W) and the reactions were carried out for 24 h. The experiments were carried out in duplicate and the absorbance was measured in triplicate.

Results and discussion

Synthesis and characterization of materials

Mesoporous aggregates of TiO_2 nanoparticles (F0) were prepared by controlled hydrolysis of titanium(IV) isopropoxide in a solution of HNO_3 in water at pH 2 following the same synthetic protocol described recently by us (Sánchez-Muñoz et al. 2013). Using an analogous synthetic method, fluorine-doped mesoporous aggregates of TiO_2 nanoparticles (F1–F10) were prepared by adding to the solution mixtures different concentrations of NaF in Milli-Q water, avoiding the use of other more expensive fluorinating reagents such as NH_4F or trifluoroacetic acid. The reactions were carried out by stirring at room temperature during 16 h and after the removal of the solvents by simple filtration and washing with water, a final calcination step was carried out at 500, 600 or 650 °C for 16 h with a heating rate of 0.8 °C/min. The resulting materials were named F0-500, F0-600, F0-650, F1-500, F1-600, F1-650, F2-500, F2-600, F2-650, F5-500, F5-600, F5-650, F10-500, F10-600 and F10-650, where 0, 1, 2, 5 or 10 is the quantity of fluorine doping, and 500, 600 and 650 are the calcination temperatures.

The resulting solids were characterized by various techniques including N_2 adsorption–desorption

isotherms, powder XRD, solid-state ^{19}F NMR spectroscopy, diffuse reflectance spectrometry and transmission electronic microscopy (TEM).

X-ray diffraction (XRD)

The XRD patterns of the TiO_2 materials show diffraction peaks assigned to the anatase phase (Fig. 1) as well as in some cases very low intensity peaks assigned to brookite and rutile (Fig. 1). The rutile phase is not present in the samples calcined at 500 °C, although it appears in the diffractograms of the materials calcined at 600 and 650 °C. The proportion of rutile increases at 650 °C, this is due to a small portion of anatase transforming to rutile with increasing temperature, due to a higher thermodynamic stability of rutile compared to anatase. However, anatase is the major component in all the synthesized materials with proportions higher than 90 % in all cases (for a detailed composition of the mixture see Table S1 of Supplementary Material).

As observed in the XRD patterns, there was a slight increase of the intensity of the peaks, associated to an increase of the crystallinity of the materials on raising the calcination temperature, and is indicative of a greater size of the studied particles compared to those samples calcined at 500 °C. There was an increase of the intensity of the (004) peaks after doping with F, which is normally associated to a slight increase of the formation of ultrareactive (001) facets (Yu et al. 2002;

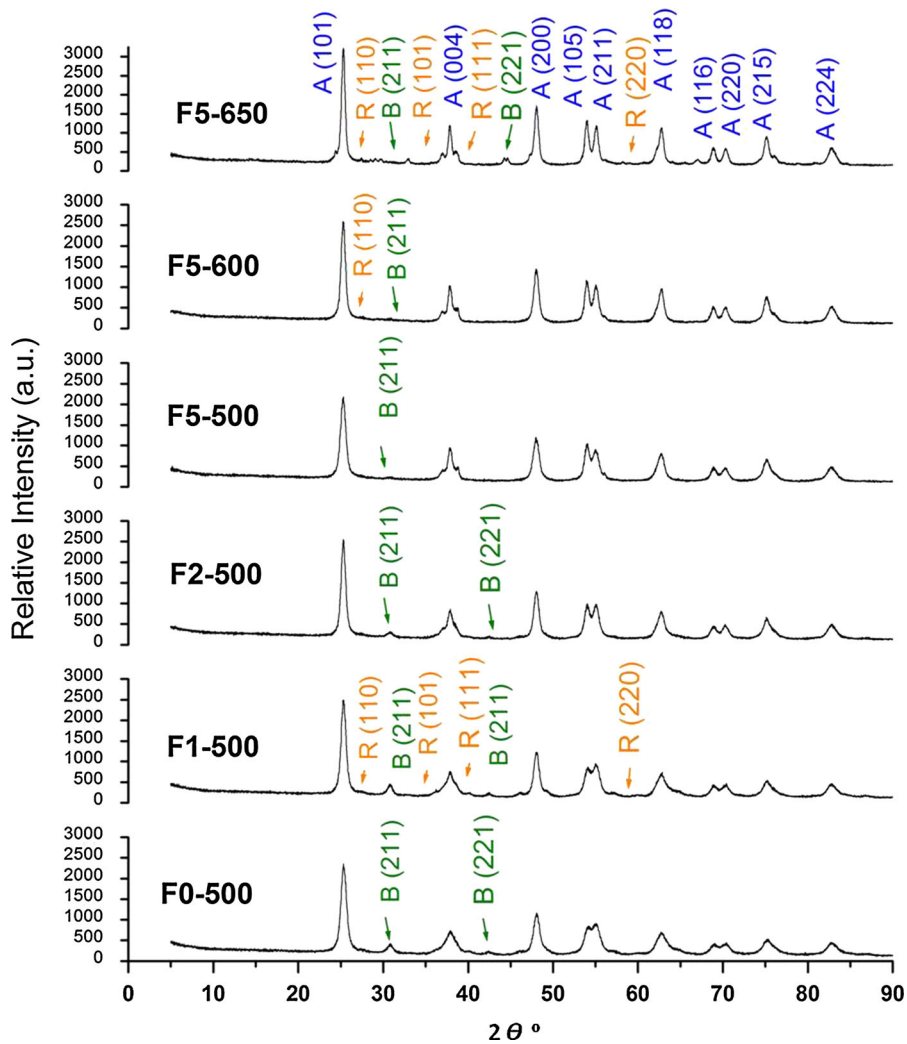

Fig. 1 X-ray diffractograms of F0-500, F1-500, F2-500, F5-500, F5-600 and F5-650

Li et al. 2005) because the (001) facets are not visible in XRD (for more details of the ratio (100):(004) peaks see Table S2 of supplementary Material). In addition, after doping with F, the position of the peaks remained almost unaltered and only a slight decrease of the crystallinity of the materials with the increase of F-doping was observed, this may be due to the fact that F can inhibit crystal growth as observed when analysing the crystallite sizes of the resulting materials (D) which were between 0.25 and 7.48 nm (Table 1) and showed a gradual decrease of the crystallite size with the increase of F-doping. It is noteworthy that the presence of fluorine influences the crystal growth process, as has been previously reported by Umadevi et al. (2014).

N_2 gas adsorption–desorption isotherms

All the synthesized materials were also characterized by nitrogen adsorption–desorption isotherms. Non-doped titanium oxide (F0-500, F0-600 and F0-650) and F-doped (1 %) materials F1-500, F1-600 and F1-650, and all the samples calcined at 500 °C show typical type IV isotherms [according to the IUPAC classification (Sing et al. 1985)] with an H2 hysteresis loop, which are indicative of the mesoporous nature of these surfaces. The other materials (F2-600, F2-650, F5-600, F5-650, F10-600 and F10-650) show typical type III isotherms with a H1 hysteresis loop (Fig. 2).

In addition, pore size distribution was obtained by applying the BJH model. The non-doped TiO_2 distributions were narrower and more homogeneous than the F-doped materials (Fig. S1 supporting information). Furthermore, pore size distribution was more heterogeneous on raising calcination temperature (Fig. S1 of supporting information).

Table 1 shows the physical parameters of nitrogen isotherms, such as BET surface area (S_{BET}), BHJ average pore diameter (d_p) and the pore volume (V_p). BET surface of all the studied materials (non-doped an F-doped TiO_2) is between 14.74 and 80.01 m^2/g and is high compared to non-porous TiO_2 materials (which usually have values between 2 and 30 m^2/g) (Mahoney and Koodaly 2014). With regards to pore diameter, all synthesized materials are in the mesoporous range (2–50 nm) with values between 6.51 and 30.06 nm. A decrease of the BET surface area, an increase of pore diameter and a slight decrease of the pore volume are associated to an increase of calcination temperature. The decrease of the porosity is due to a transformation of a part of the anatase phase into rutile, which has less surface area. In addition, with the increase of fluorine doping, BET surface area decreases and pore diameter increases. There are two

Table 1 Physical parameters of F0, F1, F2, F5 and F10 materials calcined at 500 °C measured by N_2 adsorption–desorption isotherms, X-ray diffraction and diffuse reflectance spectroscopy

Material	S_{BET} (m^2/g)	Vp (cm^3/g)	dp (nm)	D (nm)	Band gap (eV)
F0-500	80.01	0.20	6.51	*	3.06
F1-500	79.13	0.33	11.26	7.84	3.13
F2-500	51.59	0.31	16.36	2.62	3.14
F5-500	60.89	0.35	17.13	0.34	3.18
F10-500	46.27	0.21	14.49	7.83	3.16
F0-600	53.26	0.16	7.82	0.60	2.99
F1-600	44.92	0.27	15.19	0.71	3.06
F2-600	34.96	0.32	24.57	6.58	3.14
F5-600	37.92	0.36	20.84	*	3.08
F10-600	22.62	0.20	22.71	0.37	3.09
F0-650	28.85	0.11	9.25	0.78	2.94
F1-650	37.09	0.27	17.85	1.31	3.04
F2-650	25.63	0.31	26.59	*	3.15
F5-650	22.45	0.26	30.06	*	3.16
F10-650	14.74	0.18	29.32	0.71	3.17
F5-500-Pd1	62.25	0.27	18.13	0.25	2.92

* Schreer equation could not be applied

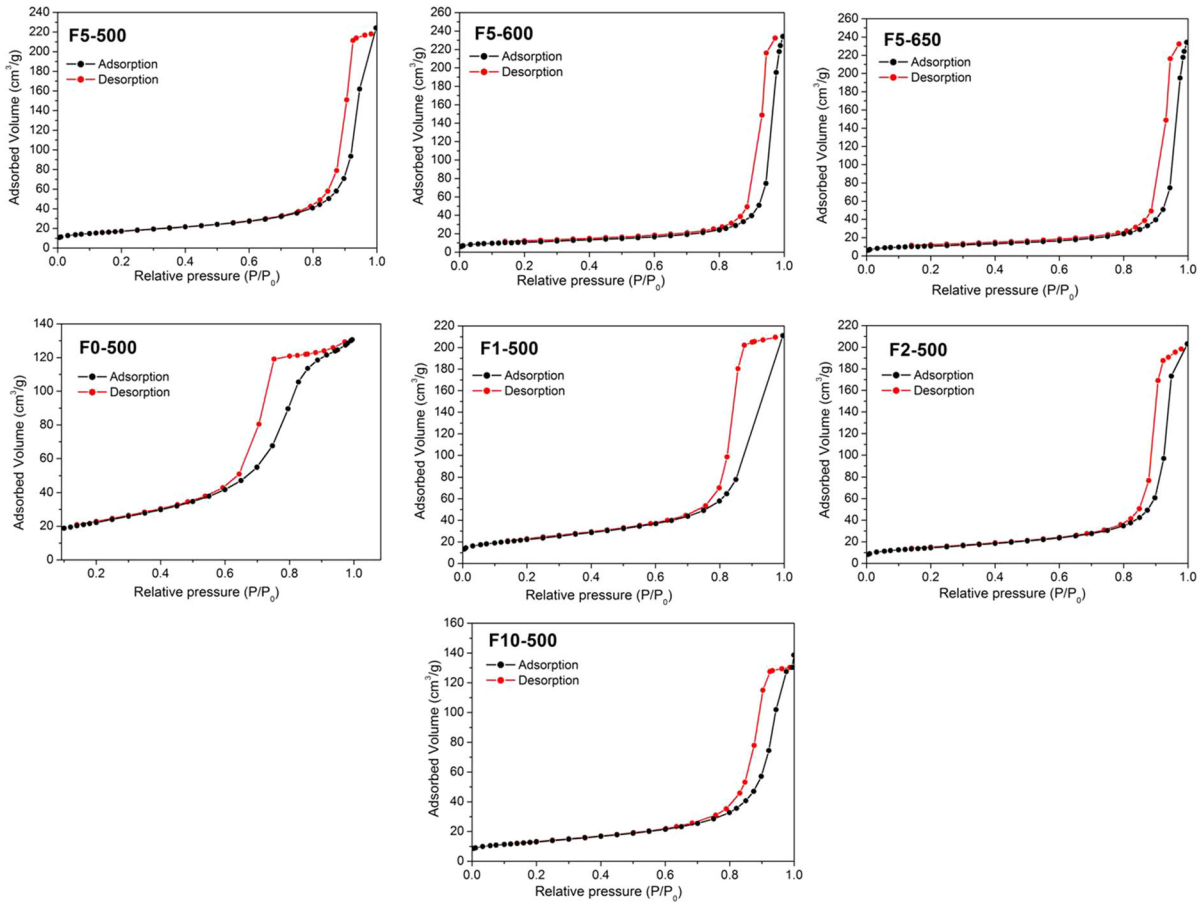

Fig. 2 Nitrogen adsorption–desorption isotherms of F0-500, F1-500, F2-500, F5-500, F10-500, F5-600 and F5-650

clear exceptions to this tendency, materials F5-500 and F5-600 which have a high BET surface area and more porosity than the rest of TiO_2 materials.

^{19}F NMR spectroscopy

F-doped materials were characterized by solid-state ^{19}F NMR spectroscopy and their spectra compared with that of NaF. In the ^{19}F NMR spectrum of NaF (Fig. 3), a single peak at around −225 ppm was observed. This signal is associated to the fluoride ions in the sodium fluoride crystalline lattice. As can be observed in the NMR spectrum of F5-500 (Fig. 3), there is an intense peak at −123 ppm and another peak with much lower intensity at −150 ppm, corresponding to the fluoride

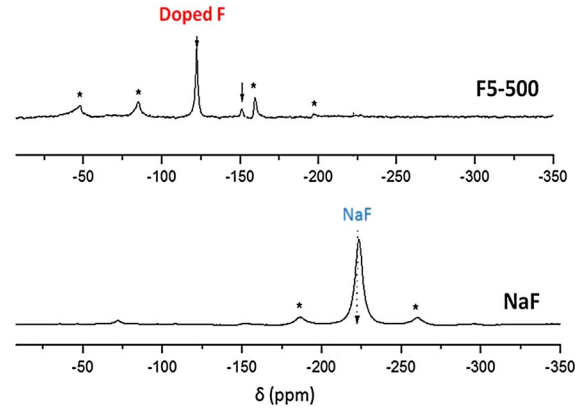

Fig. 3 ^{19}F NMR spectra of NaF and F5-500 (* =spinning side bands)

ions forming part of the doped titanium oxide structure, presumably in form of Ti–F bonds.

UV–Vis spectra

All materials were also characterized by diffuse reflectance spectroscopy (Figure S2 of Supplementary Material), and the band gap of TiO_2 samples was calculated (Fig. 4). The band gap values decrease on raising the calcination temperature (Table 1; Fig. 4). This is probably due to the increase in the quantity of rutile associated with the increase of the calcination temperature [band gap of rutile is 3.02 eV and anatase is 3.23 eV (Zaleska 2008)]. A decrease of band gap values with the increase in the quantity of fluorine is not observed, in fact, a slight increase of the band gap values was recorded.

Conventional transmission electron microscopy (TEM)

TEM has also been used for the characterization of the materials prepared (Fig. 5). The major part of the particles has a square or hexagonal form (with two edges longer than the other four). In addition, particles have a similar form to those described in the literature which have ultrareactive facets [001] (Dozzi and Selli 2013).

Particle size distribution of all the materials has also been obtained by TEM images using the software *ImageJ* (Insets Fig. 5; Table 2). Non-doping TiO_2 (F0-500) distribution is more homogeneous and has an average particle size of 10.97 ± 2.12 nm, smaller than those of the other F-doped TiO_2 materials. On the other hand, particle size distribution of titanium oxide is more heterogeneous and a gradual increase is observed on raising the calcination temperature. It is well known that when particle size is over 14 nm in the anatase phase, it begins to be transformed into rutile (Sabyrov et al. 2013). Therefore, according to the particle size distribution, a transformation of part of the anatase into rutile in F5-600 and F5-650 materials is plausible. This phenomenon was confirmed by XRD where small peaks corresponding to rutile were observed (Fig. 1).

Photocatalytic degradation of methylene blue

In this study, MB was chosen as a model pollutant for testing photocatalytic activities of the synthesized materials. Firstly, the materials were stirred in the dark during 1 h to reach the adsorption equilibrium, which was always quantified to be the adsorption of less than 5 % of MB. Subsequently, the photocatalytic degradation of MB was carried out under UV light (365 nm) irradiation from a 6 W Hg lamp for 2 h.

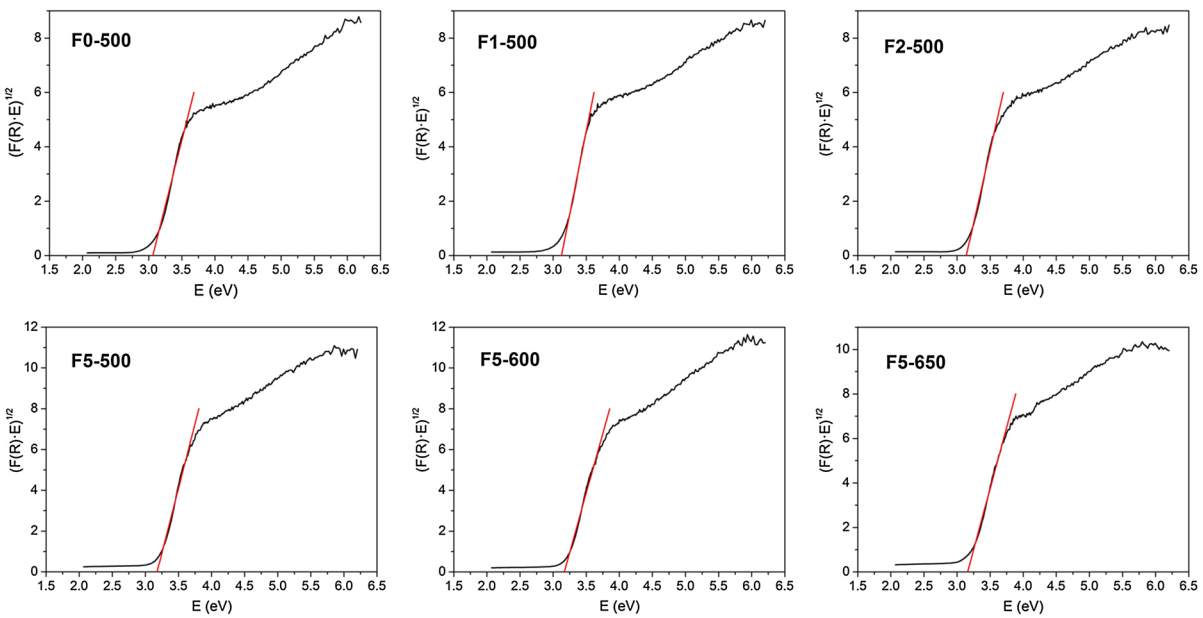

Fig. 4 Band gap calculation of F0-500, F1-500, F2-500, F5-500, F5-600 and F5-650

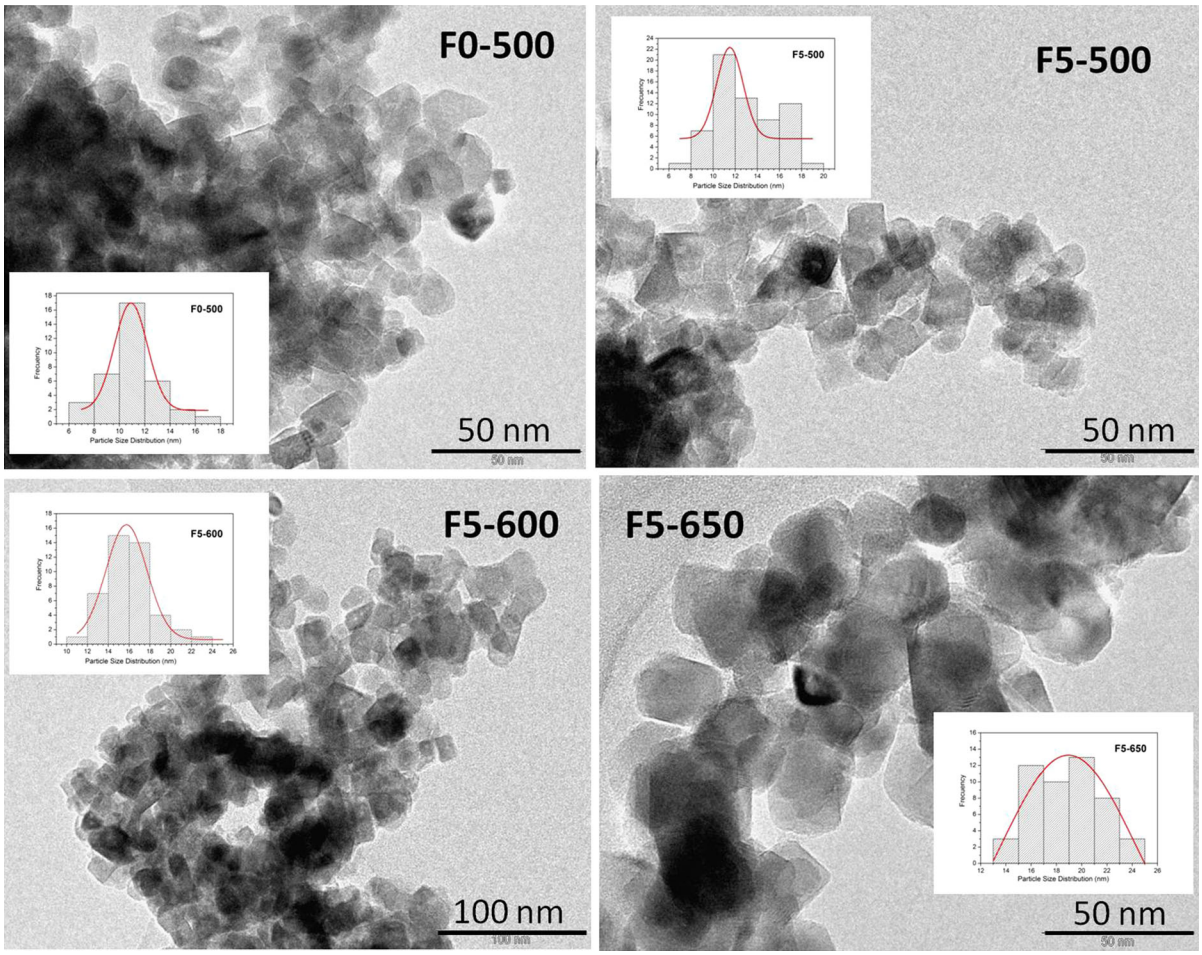

Fig. 5 TEM images of F0-500, F5-500, F5-600 and F5-650. Insets show the particle size distribution for each material

Table 2 Particle size distribution of F0-500, F5-500, F5-600 and F5-650

	Particle size distribution (nm)
F0-500	10.97 ± 2.12
F5-500	13.01 ± 2.74
F5-600	16.13 ± 2.44
F5-650	18.79 ± 2.75

To study the influence of the quantity of fluorine on the photocatalytic behaviour, 25 mg of photocatalyst was suspended in 100 mL of a 0.01 mM aqueous solution of MB. Figure 6 and Table 3 show the results obtained from this study. It seems that the degradation of MB follows first-order kinetics, in which the rate constants for the degradation (k, s^{-1}) are determined from regression curves of $\ln(C/C_0)$ versus the irradiation time. As can be observed, the values of k for the photocatalysts increase progressively with increasing quantity of F up to 5 %.

However, an exception is the F10-500 sample, which has less photocatalytic activity than the other F-doped materials. This is probably due to an excess in the fluorine doping in this material which can serve as a recombination centre with the consequent decrease in the photocatalytic activity.

The increase of photocatalytic activity with higher quantities of F is not due to the decrease of band gap values (see Table 1 which shows a slight increase of band gap values with increasing amounts of F), but probably to the presence of [001] ultrareactive facets normally formed during the synthesis of titanium oxides in fluorinated reaction mixtures and which have

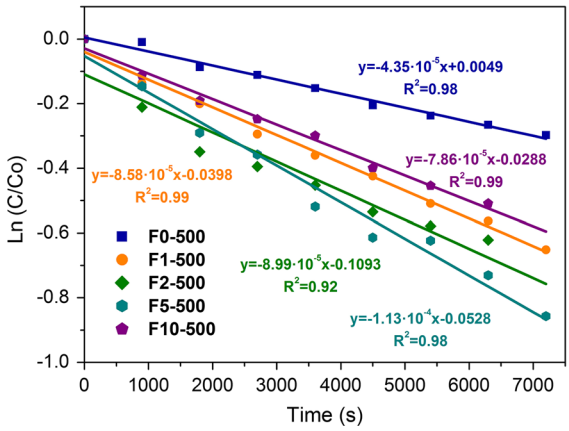

Fig. 6 Photocatalytic degradation of methylene blue with 25 mg of F0-500, F1-500, F2-500, F5-500 and F10-500

Table 3 Apparent kinetic constants (k, s^{-1}) for the degradation of MB using 25 mg of F-doped titanium oxide under UV light during 2 h

Material	k (s^{-1})
F0-500	4.35×10^{-5}
F0-600	1.23×10^{-4}
F0-650	1.39×10^{-4}
F1-500	8.58×10^{-5}
F1-600	1.32×10^{-4}
F1-650	1.21×10^{-4}
F2-500	8.99×10^{-5}
F2-600	3.71×10^{-5}
F2-650	5.70×10^{-5}
F5-500	1.13×10^{-4}
F5-600	5.77×10^{-5}
F5-650	6.49×10^{-5}
F10-500	7.86×10^{-5}

more reactivity than [101] predominant facets (Dozzi and Selli 2013). In addition, the improved photocatalytic activity may also be ascribed to the formation of Ti–F groups on the surface which can act as trapping sites for photogenerated electrons and facilitate transfer to adsorbed O_2 molecules (Yu et al. 2010).

In order to study the influence of calcination temperature, additional tests were carried out. 25 mg of photocatalyst was suspended in 100 mL of a 0.01 mM MB aqueous solution for F0 and F1 materials, and 15 mg of photocatalyst in 100 mL of a 0.02 mM MB aqueous solution for F2 and F5 materials. Materials with higher amounts of F have high photocatalytic activity, so it was necessary to change the test conditions for F2 and F5 samples. F10 tests were not carried out in detail because preliminary experiments showed that they presented less photocatalytic activity compared with the rest of the materials (Fig. 6). The results obtained are shown in Fig. 7, Fig. 8 and Table 3.

The photocatalytic activity increases on raising the calcination temperature for F0 and F1 materials. This is due to the presence of a small proportion of rutile which may favour the degradation, as normally occurs for P25 commercial titanium oxide, which is a mixture of anatase and rutile.

In F2 and F5 materials, an increase of the calcination temperature does not induce a higher photocatalytic activity, probably because the F-doping affects more the anatase than the rutile phase, the kinetic constant of F5 material calcined at 500 °C (F5-500) is higher than materials calcined at 600 or 650 °C, which have a greater proportion of rutile. In addition, it has been previously established that smaller particle size is normally associated to a more reactive material surface because of the decrease in the recombination processes (Kudo and Miseki 2009). This could be the reason why F5-500 material has higher photocatalytic activity than F5-600 or F5-650 which have a higher average particle size (Table 2). It is important to note that all studied materials have higher photocatalytic activity using the same experimental conditions than Zn-doped analogues synthesized by our group (Sánchez-Muñoz et al. 2013).

Synthesis and characterization of hybrid material F-doped TiO_2 with supported Pd nanoparticles

Hybrid F-doped TiO_2 with supported palladium nanoparticles (F5-500-Pd1) was synthesized using a grafting reaction of a palladium(II) organometallic salt [$Pd(cod)Cl_2$] onto the previously synthesized titanium oxide. The hybrid F-doped TiO_2-Pd nanoparticles (F-500-Pd1) were characterized by N_2 adsorption–desorption isotherms, powder XRD, solid-state ^{19}F NMR spectroscopy, diffuse reflectance spectrometry and TEM.

The XRD pattern of the F5-500-Pd1 shows that the hybrid material keeps the anatase structure (Fig. 9) and the crystallite size (D) is 0.253 nm (Table 1), similar to that of the material doped only with fluorine (F5-500, 0.341 nm). Nitrogen adsorption–desorption isotherm shows that F-500-Pd1 has a type III isotherm, in contrast to F5-500 (Fig. 9), which has a type IV

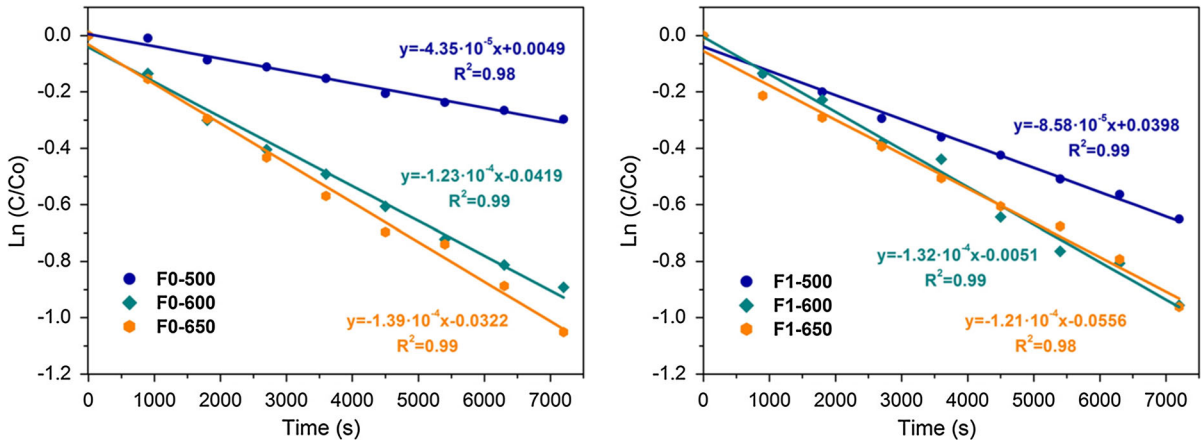

Fig. 7 Photocatalytic degradation of methylene blue with 25 mg of F0 and F1 material series

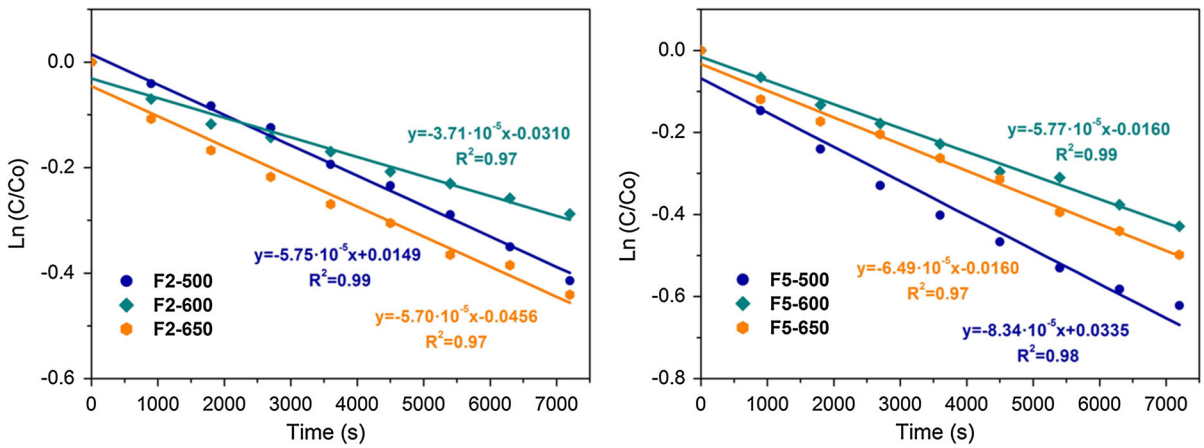

Fig. 8 Photocatalytic degradation of methylene blue with 15 mg of F2 and F5 material series

isotherm (Fig. 2). The pore diameter distribution is slightly more homogeneous than the F-doped material (Fig. S3 of supporting information). However, BET surface area, pore volume and pore diameter are similar to those of F5-500 (Table 1). Band gap value of F5-500-Pd1 is 2.92 eV (Fig. 10; Table 1), which is, as expected, much lower than that of F5-500 (3.18 eV). This decrease of the band gap has a great influence on the photocatalytic activity of F5-500-Pd1 under visible light, as described in "Photocatalytic activity of the hybrid material under visible light" section. The TEM images show that the hybrid material maintains its structural integrity with the TiO_2 nanoparticles with the same morphology and forming aggregates, on top of which are palladium nanoparticles conglomerates of around 40 nm (Fig. 11). The EDX spectrum also confirms the palladium nanoparticle presence in the hybrid material (Fig. 11).

Photocatalytic activity of the hybrid material under visible light

A photocatalytic degradation experiment using the hybrid material F5-500-Pd1 was carried out under visible LED light (4.5 W) for 24 h, instead of using UV light. Degradation of MB was observed under visible LED light (Fig. 12), with a kinetic constant of $1.32 \times 10^{-5}\ s^{-1}$. The same photocatalytic experiment was carried out using F5-500 material and no degradation of MB was observed.

The much higher photocatalytic activity of the hybrid material in comparison with F5-500 is maybe

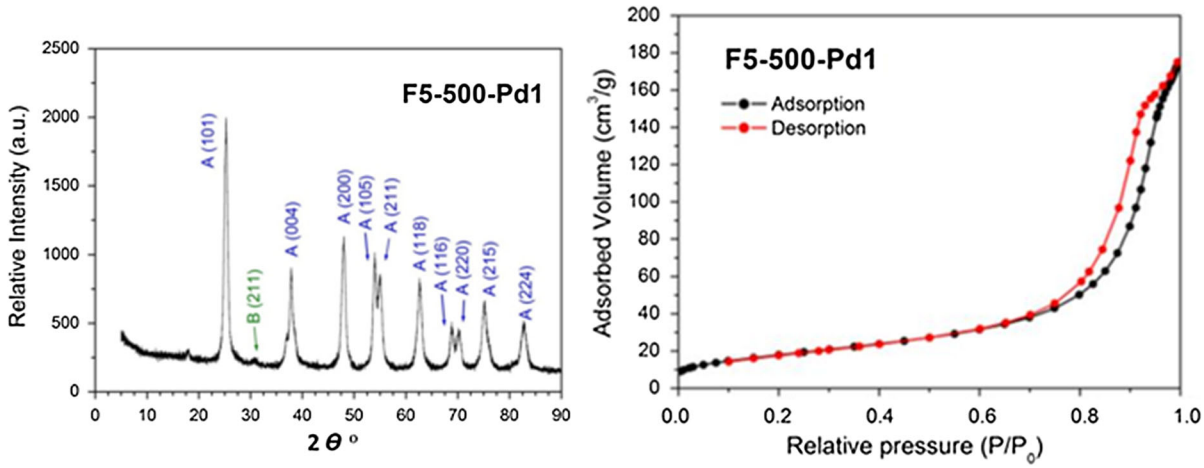

Fig. 9 X-ray diffractogram and N_2 adsorption–desorption isotherm of F5-500-Pd1

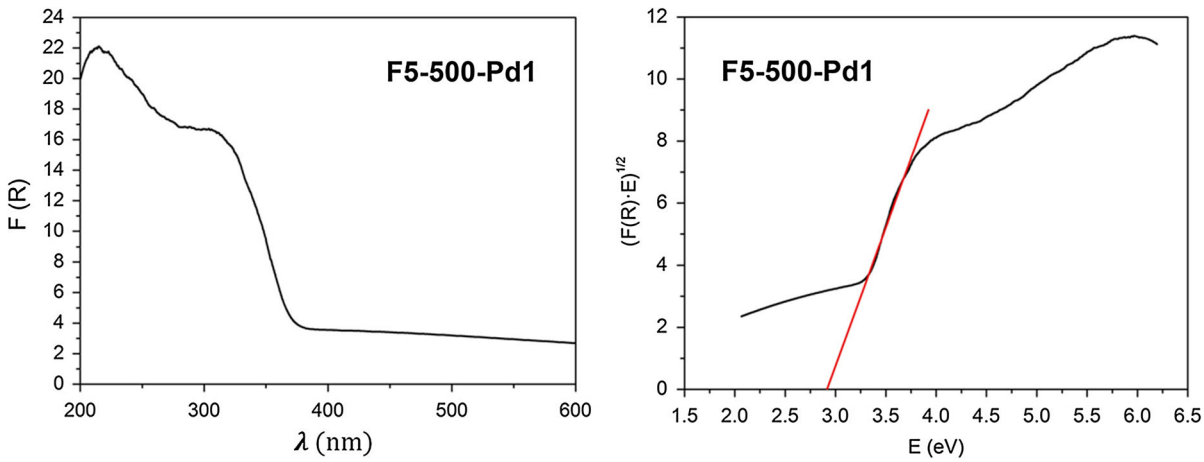

Fig. 10 Diffuse reflectance spectra and band gap calculation of F5-500-Pd1

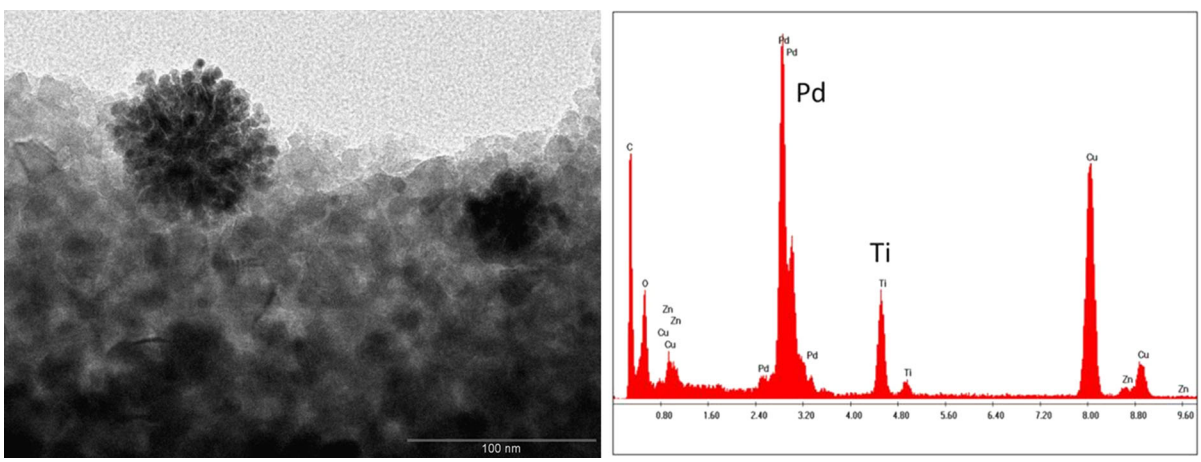

Fig. 11 TEM image and EDX spectra of F5-500-Pd1

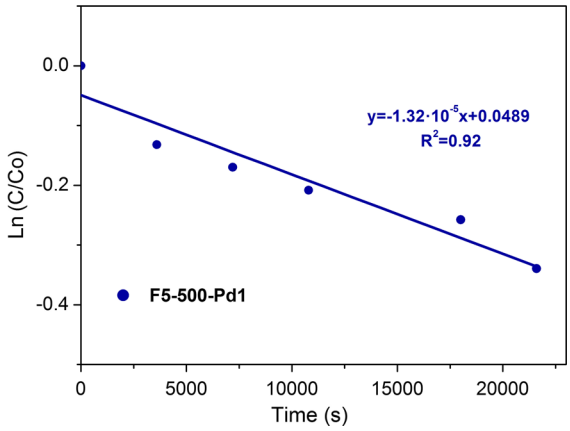

Fig. 12 Photocatalytic degradation of methylene blue with F5-500-Pd1

due to the lower band gap value of the hybrid material which is able to absorb a higher percentage of visible light to start the photocatalytic process. In addition, the higher photocatalytic activity of F5-500-Pd1 may also be due to the surface plasmon resonance effect. In addition, the palladium incorporation in the hybrid material structure may decrease the electron–hole pair recombination, supporting the degradation process and enhancing the photocatalytic activity.

Conclusions and outlook

The synthesis of non-doped and F-doped TiO_2 materials has been carried out with a simple and cheap synthetic method. The resulting materials were calcined at 500, 600 and 650 °C. Characterization has been carried out using different techniques and shows that the synthesized materials are mesoporous aggregates of nanoparticles with BET surfaces between 14.74 and 80.01 m^2/g and pore diameters between 6.51 and 30.06 nm. XRD shows that the materials principally consist of anatase and a very small proportion of brookite, additionally a very small quantity of rutile is also formed on raising the calcination temperature (from 500 to 600 and/or 650 °C). Band gap values of all resulting materials are between 2.94 and 3.18 eV and variation in the quantity of F does not produce significant changes in the band gap values.

The photocatalytic degradation of MB was carried out under UV light (365 nm) irradiation from a 6 W Hg lamp, observing a much higher photocatalytic activity of doped materials compared to the non-doped TiO_2 (F0). The apparent rate constants for the degradation of MB indicate a positive influence of the F-doping on the photocatalytic activity, even though a decrease of band gap was not observed. F5-500 is apparently the material which has the best structural properties and photocatalytic activity, due to its high crystallinity, surface area and porosity.

A hybrid material F-doped TiO_2–Pd nanoparticles (F5-500-Pd1) has been synthesized and characterized observing that most of the textural properties changed only slightly after the incorporation of the Pd nanoparticles. The only property which showed a significant change after the impregnation of the Pd nanoparticles was the band gap value which was notably lower compared with that of the parent material (F5-500). F5-500-Pd1 was used as photocatalyst for the photocatalytic degradation of MB under LED visible light (4.5 W) for 24 h, observing a kinetic constant of 1.32×10^{-5} s^{-1}. Under the same conditions, degradation of MB was not observed under LED visible light using F5-500 material which confirms the importance of lowering the band gap in the hybrid material upon the incorporation of palladium nanoparticles.

References

Bayarri B, Gimenez J, Curco D, Esplugas S (2005) Photocatalytic degradation of 2,4-dichlorophenol by TiO_2/UV: kinetics, actinometries and models. Catal Today 101:227–236

Chen X, Mao SS (2007) Titanium dioxide nanomaterials: synthesis, properties, modifications, and applications. Chem Rev 107:2891–2959

Cherchi C, Gu AZ (2010) Impact of titanium dioxide nanomaterials on nitrogen fixation rate and intracellular nitrogen storage in *Anabaena variabilis*. Environ Sci Technol 44(21):8302–8307

Cui Y, Du H, Wen L (2008) Doped TiO_2 photocatalysts and synthesis methods to prepare TiO_2 films. J Mater Sci Technol 24(5):675–689

Danilchenko SN, Kukharenko OG, Moseke C, Protsenko IY, Sukhodub LF, Sulkio-Cleff B (2002) Determination of the bone mineral crystallite size and lattice strain from diffraction line broadening. Cryst Res Technol 37:1234–1240

Diebold U (2003) The surface science of titanium dioxide. Surf Sci Rep 48:53–229

Dozzi MV, Selli E (2013) Specific facets-dominated anatase TiO_2: fluorine-mediated synthesis and photoactivity. Catalysts 3:455–485

Glaze WH, Kang JW, Chapin DH (1987) The chemistry of water treatment processes involving ozone, hydrogen peroxide and ultraviolet radiation. Ozone Sci Eng 9:335–352

Herrmann JM, Duchamp C, Karkmaz M, Hoai BT, Lachheb H, Puzenat E, Guillard C (2007) Environmental green chemistry as defined by photocatalysis. J Haz Mater 146:624–629

Hoffmann MR, Martin ST, Choi W, Bahnemannt D (1995) Environmental applications of semiconductor photocatalysis. Chem Rev 95:69–96

Jin YZ, Zhang YF, Li E (2003) Micro-electrolysis technology for industrial wastewater treatment. J Environ Sci 15:334–338

Kudo A, Miseki Y (2009) Heterogeneous photocatalyst materials for water splitting. Chem Soc Rev 38:253–278

Li D, Haneda H, Labhsetwar NK, Hishita S, Ohashi N (2005) Visible-light-driven photocatalysis on fluorine-doped TiO_2 powders by the creation of surface oxygen vacancies. Chem Phys Lett 401:579–584

Luttrell T, Halpegamage S, Tao J, Kramer A, Sutter E, Batzill M (2014) Why is anatase a better photocatalyst than rutile?—model studies on epitaxial TiO_2 films. Scientific Rep 4:4043

Mahoney L, Koodaly RT (2014) Versatility of evaporation-induced self-assembly (EISA) method for preparation of mesoporous TiO_2 for energy and environmental applications. Materials 7:2697–2746

Mohammed MA, Shitu A, Ibrahim A (2014) Removal of methylene blue using low cost adsorbent: a review. Res J Chem Sci 4:91–102

Sabyrov K, Burrows ND, Penn RL (2013) Size-dependent anatase to rutile phase transformation and particle growth. Chem Mater 25(8):1408–1415

Sami G, Bagani N (2012) Sorption kinetics for dye removal from aqueous solution using natural clay. J Environ Earth Sci 2:30–40

Sánchez-Muñoz S, Pérez-Quintanilla D, Gómez-Ruiz S (2013) Syntesis and photocatalytic applications of nano-sized zinc-doped mesoporous titanium oxide. Mater Res Bull 48:250–255

Sing KSW, Everett DH, Haul RAW, Moscou L, Pierotti RA, Rouquéol J, Siemieniewska T (1985) Reporting physisorption data for gas/solid systems with special reference to the determination of surface area and porosity. Pure Appl Chem 57:603–619

Tan YN, Wong CL, Mohamed AR (2011) An overview on the photocatalytic activity of nano-doped-TiO_2 in the degradation of organic pollutants. ISRN Mater Sci 2011:261219

Teichner SJ (2008) The origins of photocatalysis. J Porous Mater 15:311–314

Umadevi M, Parimaladevi R, Sangari M (2014) Synthesis, characterization and photocatalytic activity of fluorine doped TiO_2 nanoflakes synthesized using solid state reaction method. Spectrochim Acta A: Mol Biomol Spectro 120:365–369

Vivero-Escoto JL, Chiang YD, Wu KCW, Yamauchi Y (2012) Recent progress in mesoporous titania materials: adjusting morphology for innovative applications. Sci Technol Adv Mater 13:013003

Wang SA (2008) Comparative study of fenton and fenton-like reaction kinetics in decolourisation of wastewater. Dye Pigment 76:714–720

Yang Y, Zhang T, Le L, Ruan X, Fang P, Pan C, Xiong R, Shi J, Wei J (2014) Quick and facile preparation of visible light-driven TiO_2 photocatalyst with high absorption and photocatalytic activity. Sci Rep 4:7045

Yu JC, Yu JG, Ho WK, Jiang ZT, Zhang LZ (2002) Effects of F^- doping on the photocatalytic activity and microstructures of nanocrystalline TiO_2 powders. Chem Mater 14:3808–3816

Yu J, Xiang Q, Ran J, Mann S (2010) One-step hydrothermal fabrication and photocatalytic activity of surface-fluorinated TiO2 hollow microspheres and tabular anatase single micro-crystals with high-energy facets. CrystEngComm 12:872–879

Yue QY, Gao BY, Wang Y, Zhang H, Sun X, Wang SG, Gu RR (2008) Synthesis of polyamine flocculants and their potential use in treating dye wastewater. J Hazard Mater 152:221–227

Zaleska A (2008) Doped TiO_2: a review. Recent Pat Eng 2:157–164